Constraints on Hf and Zr mobility in high-sulfidation epithermal systems: formation of kosnarite, KZr2(PO4)3, in the Chaquicocha gold deposit, Yanacocha district, Peru

Dr. Artur P. Deditius [1,*]

Phone +61 (8) 93602525
Email A.Deditius@murdoch.edu.au

Satoshi Utsunomiya [2]

Pablo Sanchez-Alfaro [3,4]

Martin Reich [3,4]

Rodney C. Ewing [5]

Stephen E. Kesler [6]

[1] School of Engineering and Information Technology, Murdoch University, 90 South Street, Murdoch, WA, 6150 Australia

AQ1

[2] Department of Chemistry, Kyushu University, Hakozaki, 6-10-1, Higashi-ku, Fukuoka-shi, 810-8560 Japan

[3] Department of Geology, Universidad de Chile, Plaza Ercilla 803, Santiago, Chile

[4] Andean Geothermal Center of Excellence (CEGA), Universidad de Chile, Santiago, Chile

[5] Department of Geological and Earth Sciences, Stanford University, Stanford, CA, 94305-2115 USA

6 Department of Earth and Environmental Sciences, University of Michigan, Ann Arbor, MI, 48109-1005 USA

Abstract

We report the first occurrence of Hf-rich kosnarite [$K(Hf,Zr)_2(PO_4)_3$], space group *R-3c*, $Z = 6$, in the giant Chaquicocha high-sulfidation epithermal gold deposit in the Yanacocha mining district, Peru. Kosnarite crystals are small (<100 μm) and occur in 2–3-mm-thick veins that cut intensively silicified rocks. The paragenesis includes a first stage of As-free pyrite and quartz (plus gratonite and rutile), followed by trace metal-rich pyrite [$(Fe,As,Pb,Au)S_2$] and secondary Fe-sulfates. Kosnarite is associated with quartz and is clearly late within the paragenetic sequence. Electron microprobe analyses (EMPA) of kosnarite show relatively high concentrations of HfO_2 and Rb_2O (7.61 and 1.05 wt.%, respectively). The re-calculated chemical formulas of kosnarite vary from $K_{\Sigma 1.00}(Zr_{1.93}Na_{0.01}Hf_{0.01}Mn_{0.01})_{\Sigma 1.96}(P_{3.04}O_4)_{\Sigma 3}$ to $(K_{0.92}Rb_{0.05}Na_{0.03})_{\Sigma 1.00}(Zr_{1.81}Hf_{0.19})_{\Sigma 2.00}[(P_{2.98}Si_{0.02}As_{0.01})_{\Sigma 3.01}O_4]_{\Sigma 3}$, where Hf and Rb are most likely incorporated according to a coupled substitution of $Hf^{4+} + Rb^{+} \Leftrightarrow Zr^{4+} + K^{+}$. Back-scattered electron (BSE) images and elemental mapping of kosnarite reveal that Hf and Rb are enriched in 2–10-μm-wide oscillatory and/or sector zones. High-angle annular dark-field scanning transmission electron microscopy (HAADF-STEM) observations of such zones reveal a pattern of alternating, 5–50-nm-thick, Hf-rich and Zr-rich nanozones. These high-resolution observations indicate that the incorporation of Hf does not appear to cause significant distortion in the kosnarite structure. Semiquantitative TEM-energy-dispersive X-ray spectrometry (EDS) analyses of the nano-layers show up to 22 wt.% of HfO_2, which corresponds to 31 mol% of the hypothetical, $KHf_2(PO_4)_3$, end-member. The presence of kosnarite in the advanced argillic alteration zone at Yanacocha is indicative of Hf and Zr mobility under highly acidic conditions and points towards an unforeseen role of phosphates as sinks of Zr and Hf in high-sulfidation epithermal environments. Finally, potentially new geochronological applications of highly insoluble vein kosnarite,

including Rb-Sr dating, may provide further age constraints in pervasively altered areas where other isotopic systems might have been reset.

AQ2

AQ3

Nh|zrugv

Kosnarite
Chaquicocha
Yanacocha
Hafnium
Zirconium
Phosphate

Editorial handling: R. Linnen

Introduction

AQ4

High field strength elements (HFSE), including Zr, Hf, Nb, Ta, U, Th, and the rare earth elements (REEs) are generally incompatible in magmatic-hydrothermal systems and typically concentrate in accessory phases such as zircon. Despite the fact that they are relatively insoluble in most hydrothermal fluids and considered immobile, there is abundant evidence that these elements are mobile in aqueous fluids with specific hard ligands such as phosphate $(PO_4)^{3-}$, among others (Linnen et al. 2014). In this paper, we report the first occurrence of the Hf-rich zirconium phosphate kosnarite $[K(Hf,Zr)_2(PO_4)_3]$ in the giant Chaquicocha high-sulfidation epithermal gold deposit, Yanacocha district, Peru, and provide mineralogical evidence of Hf and Zr mobility in high-sulfidation epithermal systems. Kosnarite is believed to form only in pegmatitic environments during hydrothermal alteration of primary zircon, apatite, and other Zr-bearing minerals (More et al. 1983; Brownfield et al. 1993; Birch et al. 1994, 1995; Huminicki and Hawthorne 2002). Previous studies have confirmed the importance of aluminum-sulfate-phosphates (ASP) as minerals limiting the mobility of phosphorus during dissolution of primary apatite under highly acidic

conditions, generally pH <4 (Dill 2003). However, no secondary Zr- and/or Hf-rich minerals have been reported to form after dissolution of primary and accessory silicates such as zircon in extensively hydrothermally altered rocks. This paper combines mineral chemistry data, high-resolution observations, and thermodynamic modeling to confirm that kosnarite at Yanacocha is a sink for Hf and Zr in the advanced argillic alteration zone.

The Yanacocha district

The Yanacocha district straddles a portion of the continental divide in the high Andes of northern Peru and consists of eight large high-sulfidation epithermal gold deposits hosted by intense acid-leached and quartz-rich alteration in the Miocene Yanacocha Volcanic Complex. Ages of volcanism and hydrothermal advanced argillic alteration are well documented, and eruptions spanned ~6 million years from 14.5 to 8.4 Ma interspersed with discrete pulses of hydrothermal alunite from 13.6 to 8.2 Ma (Longo et al. 2010). Gold-bearing ore at Yanacocha is associated with intense quartz-rich, advanced argillic alteration in andesitic to dacitic subvolcanic domes, dikes, and pyroclastic rocks. The hydrothermal advanced argillic alteration assemblage is characterized by vuggy and granular quartz, alunite, pyrophyllite, ±dickite, ±kaolinite, and gold-bearing ores contain pyrite, covellite, enargite-digenite, tennantite, and coarse visible gold intergrown with barite, boitriodal limonite, and quartz in vugs and fractures (Longo et al. 2010).

AQ5

Chaquicocha is one of the Yanacocha gold deposits, 1700 t of Au, located in the central part of the district. This deposit developed along near-vertical fracture zones in breccia and as stratiform bodies in acid-leached pyroclastic rocks below a barren “steam-heated” granular silica cap (Longo 2000; Teal and Benavides 2010). Gold ore is hosted by quartz-rich alteration with pyrite, enargite, tennantite, covellite, minor amounts of Pb-sulfides, and native gold (Deditius et al. 2008; Longo et al. 2010; and references therein). Local zones with bonanza-grade gold ore host native gold in silica-oxide breccia and vuggy quartz intergrown with barite and limonite (Longo 2000).

AQ6

Samples and methods

Kosnarite was found in a fragment of a drill core from the Chaquicocha mine (CHQ-470/N4—depth, 343 m) in the Chaquicocha gold deposit in the Yanacocha district, Peru. The sample was examined in hand specimen, polished thin sections, and polished bulk samples by optical and scanning electron microscopy (SEM, Hitachi S3200N equipped with energy-dispersive X-ray spectrometry, EDS). The chemical composition of kosnarite was quantitatively determined by an electron microprobe analyzer (EMPA, Cameca SX100) using wavelength-dispersive spectroscopy (WDS) at the Electron Microbeam Analysis Laboratory (EMAL) at the University of Michigan. Accelerating voltage and beam current were 15 kV and 10 nA, respectively. The data acquisition time was 40 s (20 s on the peak and 10 s on each of the background positions) and spot ~1 μm analyses were performed. In order to increase the analytical total, the time of acquisition for Hf was set to 60 s. For F and Na, counting time of 20 s (10 s on the peak and 5 s on each of the background positions) and raster 5 μm were used to avoid Na and F migration under the beam. The PAP correction procedure was used to calculate the analyses. The standards used for calibration and detection limits (in ppm) are given in parenthesis: zircon ($ZrSiO_4$) for Zr(L_α) (4292) and Hf (M_α) (697), synthetic $KTaO_3$ for K (K_α) (305), $CePO_4$ for P(K_α) (1183) and Ce(L_α) (1184), pollucite for Rb (L_α) (510) and Cs (L_α) (844), albite for Al(K_α) (165) and Na(K_α) (349), $CaTiO_3$ for Ti(K_α) (384), andradite for Si(K_α) (312) and Fe(K_α) (493), manganotantallite for Mn (K_α) (486), arsenopyrite for As(L_α) (390), and Evans apatite for F(K_α) (745).

AQ7

High-resolution transmission electron microscopy (HRTEM), analytical electron microscopy (AEM), and high-angle annular dark-field scanning transmission electron microscopy (HAADF-STEM) were conducted using a JEOL JEM2010F at EMAL. HAADF-STEM images provided submicron Z-contrast resolution (in a way analogue to BSE images were obtained using EMPA/SEM). Analytical parameters/conditions were spherical aberration coefficient C_s = 1.0 mm, probe size = 1.0 nm

(STEM mode), and collection angle of the HAADF detector = 50 –110 mrad. The size of condenser aperture was 20 μm. Samples were cut out of the thin sections and mounted on the 3-mm-diameter Cu grid. Subsequently, samples were polished using tripod method and the final thinning was performed by milling with an Ar ion beam (4.0 keV) in a Gatan precise ion-polishing system.

Speciation and stability diagrams were computed with the Geochemist's Workbench® (Bethke 1996) using the SUPCRT92 data compilation (Johnson et al. 1992) complemented for Zr aqueous species and mineral phases with the chemical thermodynamics of zirconium (Brown et al. 2005) that critically reviews most of the thermodynamic Zr database available.

Mineral paragenesis and the chemical composition of kosnarite

Euhedral crystals of kosnarite occur in 2–3-mm-wide veins that cut an intensively silicified rock. These 10–100-μm crystals of kosnarite coexist with the pre-existing minerals like quartz, rutile, pyrite, Au-bearing arsenian pyrite, and Fe-sulfates (Fig. 1a). The observed paragenetic sequence was determined for one sample of drill core and it is as follows: (1) $pyrite_1$ + $quartz_1$ + gratonite [$Pb_9As_4S_{15}$], (2) As-$pyrite_2$ [$(Fe,As,Pb,Au)S_2$], (3) kosnarite + $quartz_2$, and (4) Fe-sulfates. $Pyrite_1$ pre-dates Au and most probably precipitated during quartz-alunite event (though, no alunite was found in the sample). Two generations of quartz were found in the sample, anhedral $quartz_1$ and euhedral $quartz_2$. The latter one formed in the pores and is most probably contemporaneous with kosnarite. However, the distinction between these two generations of quartz is not always straightforward, particularly in thin section. No porcelaineous-textured silica was found in the sample. The back-scattered electron (BSE) images show three different types of Hf-rich zoning in the crystals of kosnarite: (i) fine, oscillatory zoning; dominant in the samples; (ii) crystallographically oriented sector zones that mimic the terminating faces of the prism; and (iii) irregularly distributed grains with patchy-type zoning (Fig. 1a–d).

Fig. 1

Back-scattered electron (BSE) images of kosnarite (kos) and associated minerals. **a** Euhedral aggregates of kosnarite crystals deposited on the surface of quartz (qtz). Note the platy crystals of secondary Fe-sulfates (szomolnokite?) forming at the expense of porous arsenian pyrite (As-py) and gratonite (g). **b** Hf-rich patchy zoning in kosnarite formed on the surface of pyrite (py) and arsenian pyrite. **c** Fine, oscillatory Hf-rich zoning in kosnarite (*white arrows*). **d** BSE image of Hf sector zoning in kosnarite associated with elemental map of Hf (d1)

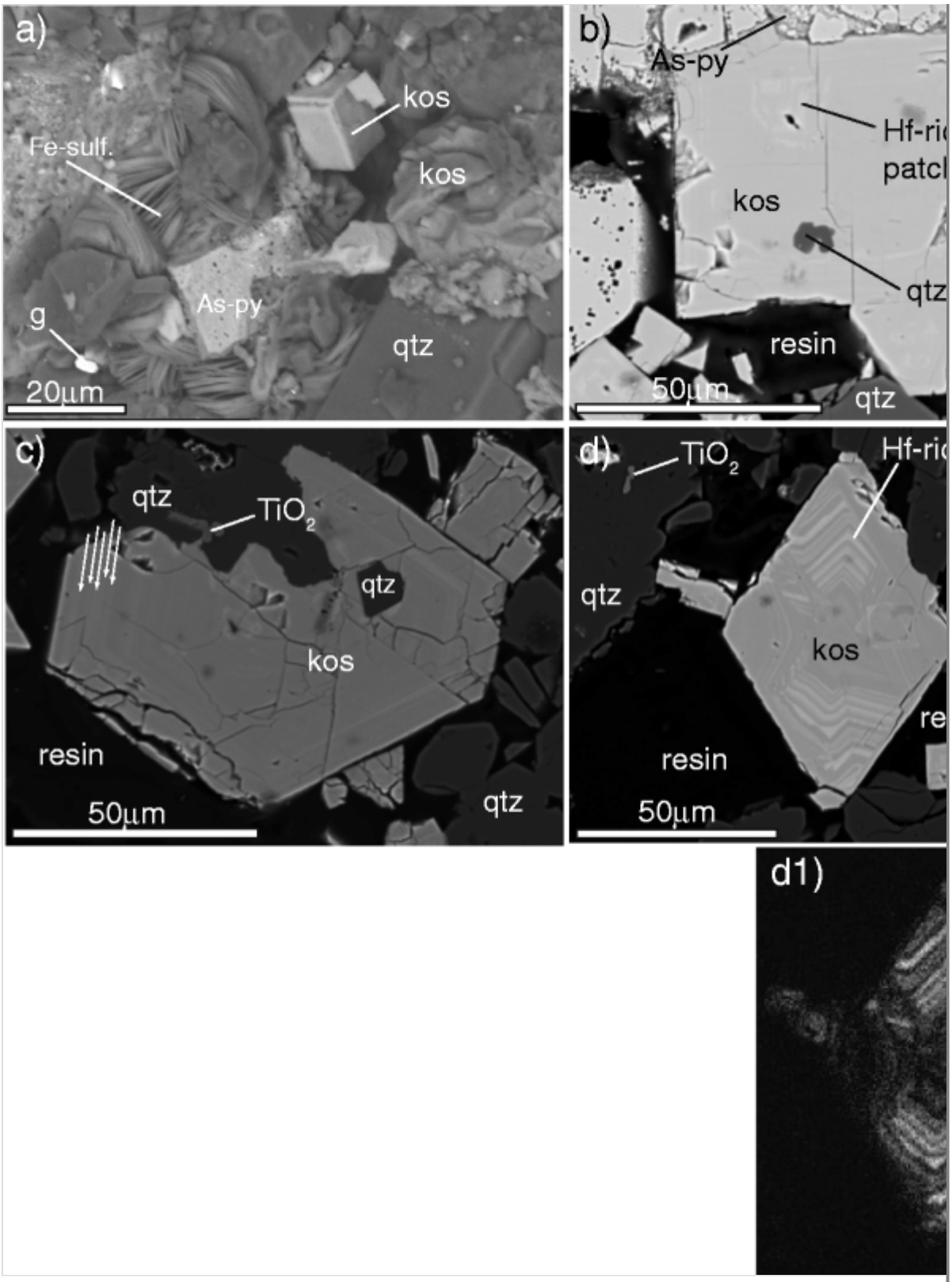

The EMPA analyses of kosnarite from the Chaquicocha deposit at Yanacocha show relatively high concentrations of HfO_2 and Rb_2O at 7.61 and 1.05 wt.%, respectively. The concentrations of other detected elements are ≤0.27 wt.% As_2O_5, ≤0.23 wt.% TiO_2, ≤0.22 wt.% Na_2O, ≤0.17 wt.% Al_2O_3, ≤0.10 wt.% FeO, and ≤0.05 wt.% MnO,

respectively. The concentrations of F, Cs_2O, and Ce_2O_3 are below detection limits (bdl) (Table 1). The re-calculated chemical formulas of kosnarite vary from (with 1σ standard deviation) $(K_{1.00}Na_{0.01})_{\Sigma 1.01\pm 0.04}(Zr_{1.93}Hf_{0.01}Mn_{0.01})_{\Sigma 1.95\pm 0.02}(P_{3.04\pm 0.15}O_4)_3$ to $(K_{0.92}Rb_{0.05}Na_{0.03})_{\Sigma 1.00\pm 0.04}(Zr_{1.81}Hf_{0.19})_{\Sigma 2.00\pm 0.02}[(P_{2.98}Si_{0.02}As_{0.01})_{\Sigma 3.01\pm 0.02}O_4]_3$. Based on the EMPA data, it is likely that Hf was incorporated into kosnarite according to coupled substitution: $Hf^{4+} + Rb^{+} \Leftrightarrow Zr^{4+} + K^{+}$. Additional, minor isovalent substitutions include, e.g., $P^{5+} \Leftrightarrow As^{5+}$ and $K^{+} \Leftrightarrow Na^{+}$. It is important to note that Hf and Rb are heterogeneously distributed: EMPA analyses, BSE images, and elemental mapping reveal that these elements are enriched in oscillatory or sector zones between 2 and 10 μm thick, as shown in Fig. 1b–d.

Table 1

Representative analyses of kosnarite from Chaquicocha

AQ9

Analyses	Det. Lim. (ppm of element)	1	2	3	4	5	6
P_2O_5 (wt.%)	1183	40.51	40.02	40.90	41.77	41.25	42.10
As_2O_5	390	0.27	0.21	n.a.	0.13	bdl	n.a.
Al_2O_3	165	bdl	0.03	bdl	bdl	bdl	bdl
SiO_2	312	0.19	0.08	bdl	0.03	bdl	bdl
TiO_2	384	bdl	0.05	bdl	bdl	bdl	bdl
ZrO_2	4292	42.79	44.18	44.15	44.45	45.72	45.00
HfO_2	697	7.61	6.90	6.20	5.60	4.75	3.84
FeO	493	0.06	bdl	bdl	bdl	bdl	0.13
Na_2O	349	0.10	0.09	0.13	0.05	0.07	0.10
K_2O	305	8.28	8.37	8.62	8.75	8.93	8.94
MnO, Ce_2O_3, Cs_2O, and F are below detection limits 486, 1184, 844, and 745, r recalculated per 12 oxygen atoms							
apfu atom per formula unit							

Analyses	Det. Lim. (ppm of element)	1	2	3	4	5	6
Rb_2O	510	0.80	0.73	1.05	0.58	0.81	0.70
Total		100.64	100.66	101.05	101.36	101.53	100.81
P [apfu]		2.975	2.946	2.983	3.007	2.977	3.024
As		0.012	0.010	n.a.	0.006	bdl	n.a.
Al		bdl	0.003	bdl	0.001	bdl	bdl
Si		0.016	0.007	bdl	0.002	bdl	bdl
Ti		bdl	0.003	bdl	bdl	bdl	bdl
Zr		1.810	1.873	1.855	1.843	1.900	1.862
Hf		0.188	0.171	0.153	0.136	0.116	0.093
Fe		0.004	bdl	bdl	bdl	bdl	0.009
Na		0.028	0.025	0.035	0.012	0.018	0.026
K		0.916	0.929	0.947	0.950	0.972	0.968
Rb		0.045	0.041	0.058	0.032	0.044	0.038
sum		5.996	6.008	6.031	5.989	6.027	6.020
MnO, Ce_2O_3, Cs_2O, and F are below detection limits 486, 1184, 844, and 745, r recalculated per 12 oxygen atoms							
apfu atom per formula unit							

AQ8

Kosnarite from the Chaquicocha deposit contains the highest amounts of Hf and Rb reported in the literature, significantly higher than kosnarite samples from pegmatites at Mount Mica, Black Mountains (USA), and Wycheproof (Australia). The maximum concentrations in oxides of Hf and Rb in the North-American pegmatites reach 1.4 and 0.3 wt.%, respectively (Brownfield et al. 1993), while slightly higher HfO_2 amounts of 1.7 wt.% were reported in the aforementioned Australian locality (Birch et al. 1994). The Hf-rich kosnarite reported in this study contains much lower concentrations of Mn and Na,

compared with kosnarite from Mount Mica, which are up to 1.3 MnO and 1.7 wt.% Na_2O, respectively.

Nanoscale Hf zoning in kosnarite

The HAADF-STEM images reveal that the individual 2–10-μm-thick oscillatory zoning identified by EMPA-BSE imaging consists of a set of alternating Hf-rich and Zr-rich nanozones with thickness varying between 1 and 50 nm (Fig. 2a, c). Some of the alternating Hf-rich and Zr-rich nanozones grew epitaxially on Zr-rich kosnarite that host inclusions of quartz (Fig. 2a). The semiquantitative TEM-EDS analyses of the individual nanozones reveal significant differences in elemental concentrations (Fig. 2c). The EDS analyses show concentrations of Hf as high as 22 wt.% of HfO_2, and within Hf-rich nanozones, Hf concentrations can be three times higher than the EMPA analyses. The Zr-rich, Hf-poor nanozones contains 7 wt.% of HfO_2, which is equivalent to the highest values obtained by EMPA analyses. This discrepancy is most probably due to the contamination of the excitation volume of the EMPA beam by submicron size Zr-rich zones. The combination of the HRTEM observations and EDS analyses of the areas next to the boundary between these two sets of nanozones (Fig. 2c–f) reveal that there is no detectable structural misfit or misorientation between the nanozones, in spite of significant differences in their chemical composition (Fig. 2e, f). Selected area electron diffraction (SAED) patterns across the nanozones reveal the single-crystal structure of kosnarite with sharp diffraction maxima (Fig. 2e).

Fig. 2

TEM images of nanozoning domains in kosnarite. **a** Hf-rich zone in the kosnarite matrix. Note the partial dissolution and replacement of Hf-rich area by Hf-depleted kosnarite. **b** Crystal boundary between Hf-rich and Zr-rich areas of kosnarite, patchy type of zoning. **c**, **d** TEM and HAADF-STEM images of kosnarite associated with the EDS spectra shown in image **c**. Note the position of the EDS analyses on the TEM image. **e** TEM image of the boundary between Hf-rich and Zr-rich zones. **f** HRTEM image and SAED pattern (*inset*, *lower right*) of the boundary between Hf and Zr zones (*magnified area* from **e**). No visible structural distortion is observed

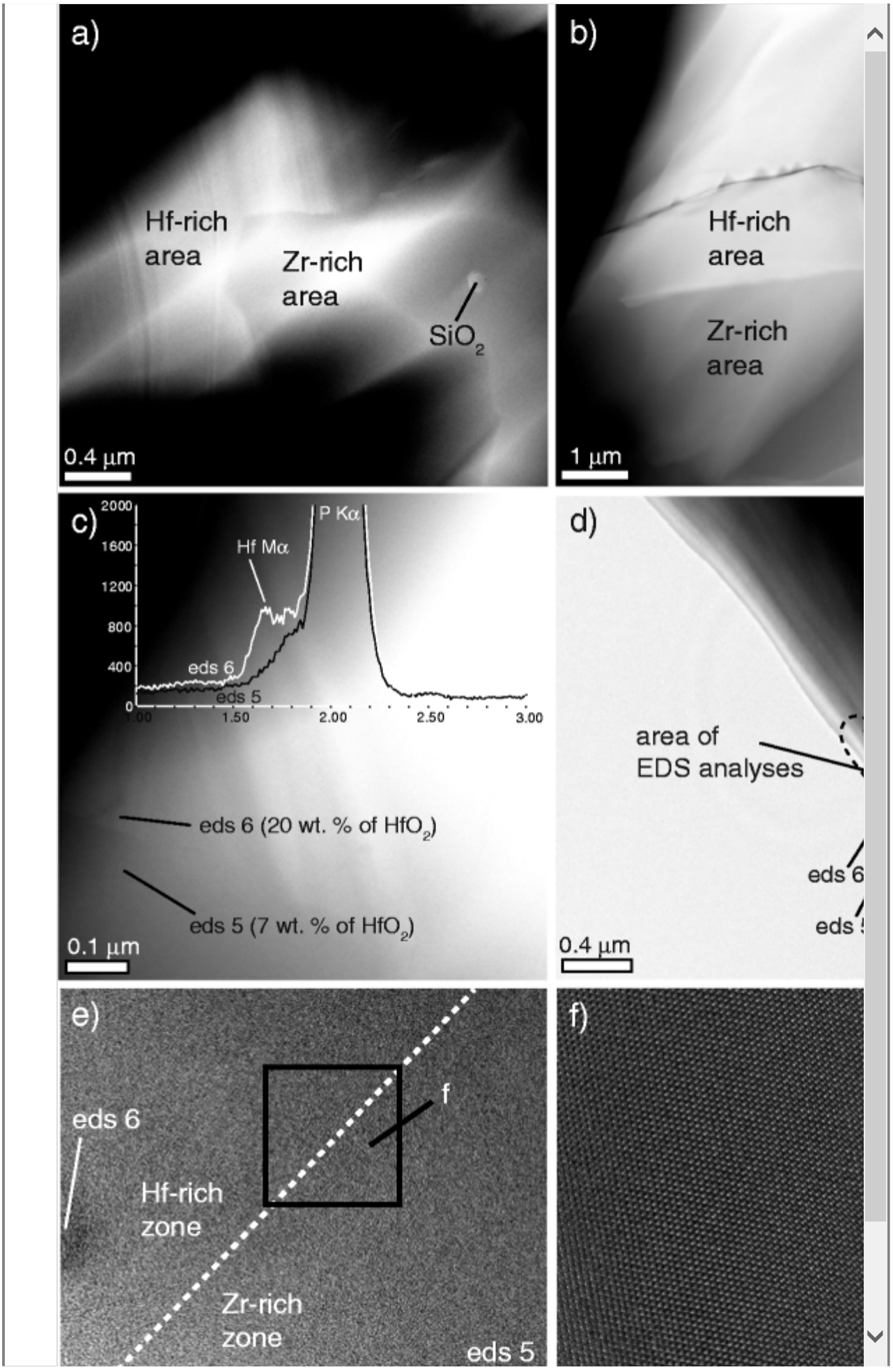
a)
Hf-rich area
Zr-rich area
SiO2
0.4 µm
b)
Hf-rich area
Zr-rich area
1 µm
c)
2000
1600
1200
800
400
0
1.00
1.50
2.00
2.50
3.00
Hf Mα
P Kα
eds 6
eds 5
eds 6 (20 wt. % of HfO2)
eds 5 (7 wt. % of HfO2)
0.1 µm
d)
area of EDS analyses
eds 6
eds 5
0.4 µm
e)
eds 6
f
Hf-rich zone
Zr-rich zone
eds 5
f)

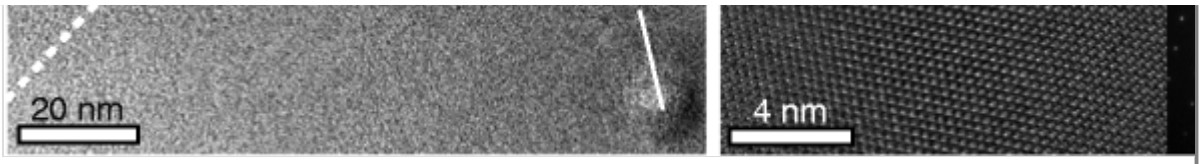

Discussion and implications

The presence of Hf-rich kosnarite in veins that cut massive silica and in voids of vuggy quartz is an evidence of mobilization and subsequent sequestration of Hf and Zr during extensive alteration of the volcanic rocks under acidic conditions, during intense quartz-rich advanced argillic alteration that hosts the high-sulfidation epithermal gold deposit at Chaquicocha. In contrast to pegmatitic environments, where kosnarite is contemporaneous with (Li,Be,Al,Ca)-hydrated secondary phosphates and Zr-bearing secondary phosphates (Brownfield et al. 1993; Birch et al. 1994, 1995), kosnarite from Chaquicocha coexists only with quartz (Fig. 1). The presence of earlier mineral assemblages in the analyzed samples, including Au-bearing As-pyrite and inclusions of fine-grained rutile in quartz (Fig. 1), suggests that kosnarite precipitated after the formation of quartz-rich advanced argillic alteration, massive quartz, and later Au deposition (cf., Longo et al. 2010). Because no relics of primary silicates and phosphates were found in the analyzed samples, it is plausible that Zr, Hf, P, K, and Rb were sourced from primary (Al)-silicates, apatite, and zircon after dissolution under acidic conditions, pH <4, characteristic for high-sulfidation epithermal deposits (Simmons et al. 2005). Consequently, the transport of chemical components throughout a network of fractures would lead to subsequent precipitation from aqueous fluids supersaturated with respect to kosnarite. Thermodynamic modeling based on the Brown et al. (2005) database indicates that the formation of kosnarite is controlled by physicochemical properties of the fluid that involves low pH conditions (<5); high contents of HPO_4^{2-} (log a[HPO_4^{2-}] >15) that decrease with temperature; dominant Zr-OH complexes; low activities of F and Ca, log a[Ca^{2+}] ≤−15 and log a[F^-] ≤−5; and decreasing temperature (Fig. 3a). It is likely that the high content of HPO_4^{2-} can only be reached locally in epithermal conditions and might be the limiting condition for the formation of kosnarite. Based on the result of the thermodynamic modeling, the higher concentrations of Ca and F in the

hydrothermal fluid would promote precipitation of (CaF)-apatite instead of kosnarite. Our thermodynamic modeling is consistent with EMPA analyses showing concentrations of F in kosnarite below the detection limit for this element (745 ppm). Therefore, it is suggested that F was not a major ligand that enhanced migration of the relatively immobile Zr and Hf, a feature that was noted in other hydrothermal systems (Rubin et al. 1993). However, the presence of $ZrF(OH)_3$ and $ZrF(OH)_2$ complexes (Magdisov et al. 2011) cannot be ruled out. Moderately hard ligands like PO_4^{3-} could also complex Zr and Hf to facilitate their transport particularly under lower pH <4 and lower temperature conditions, <200 °C (Linnen et al. 2014).

Fig. 3

Activity-pH diagrams showing stability conditions for **a** kosnarite and crystalline **b** $FeSO_4$. **a** The log a[HPO_4^{2-}] vs. pH diagram shows an expansion of the stability field of kosnarite when temperature decreases from 170 °C (*bright gray*) to 100 °C (*dark gray*). This change occurs at the expense of whitlockite and $H_3P_2O_7^-$ and $H_2P_2O7^{2-}$ aqueous species. *Dashed lines* show the stability fields of aqueous phosphate species. **b** Log fO_2 vs. pH diagram showing the stability field for $FeSO_4$ (approximating stability field of szomolnokite) and other Fe-bearing species. The stability of $FeSO_4$ (c) expands with increase of sulfate activity. The minor shifts in the stability fields of pyrite and hematite were omitted for clarity. The *dashed lines* denote the stability of S species. Magnetite disappears when S concentration is increased. Stability diagram calculations are based on the review of the thermodynamic data base of zirconium and its compounds (Brown et al. 2005), where kosnarite stability field is approximated to $Zr(HPO_4)_2 \cdot H_2O$

AQ10

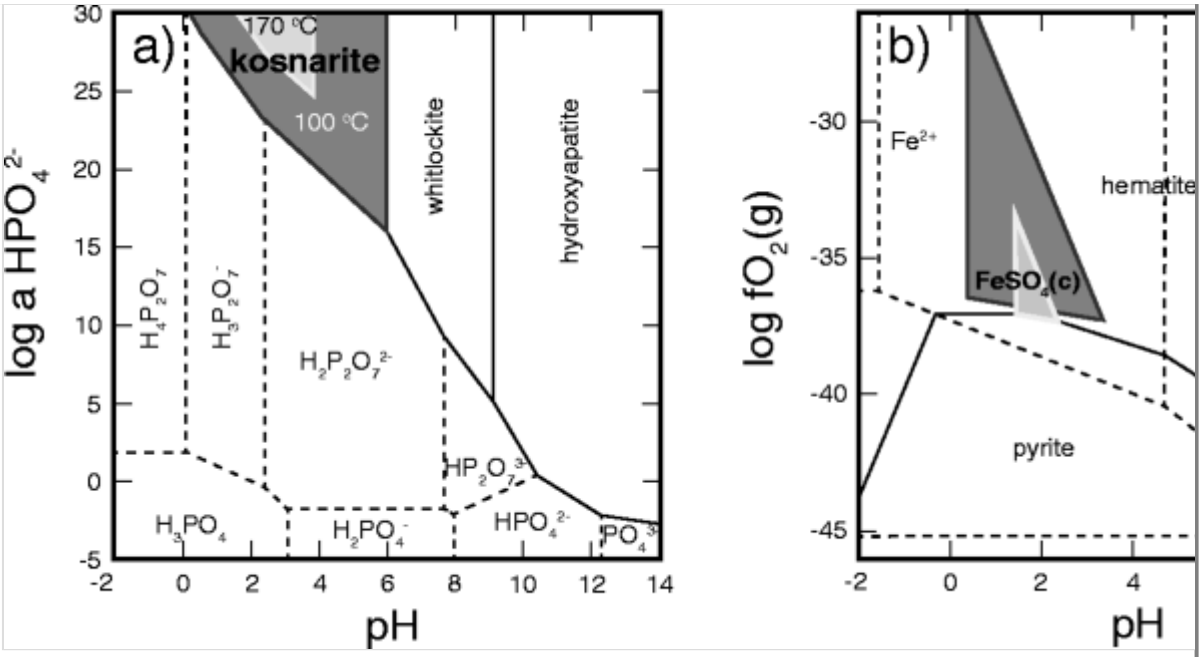

The presence of Fe-sulfates (Fig. 1) suggests that SO_4 complexes could also facilitate the transport of Zr and Hf, particularly under acidic, pH <4, and oxidizing conditions ($\log fO_2 > -32$) (Rubin et al. 1993; Aja et al. 1995), although geochemical modeling indicates that the dominating Zr species are hydroxides such as $Zr(OH)_n$ (Brown et al. 2005). Formation of crystalline $FeSO_4$ is promoted by relatively high S concentrations ($\log a[SO_4^{2-}] \geq 0.5$) (Fig. 3b), which are much higher than $\log m[SO_4^{2-}] = -2$, as proposed for szomolnokite by Chouinard et al. (2005). The conditions of kosnarite formation presented here are in agreement with those reported for aluminum-sulfate-phosphate (ASP) precipitation, formed in the vicinity of the feeder systems of epithermal gold and porphyry deposits (Dill 2003; and references therein).

The presence of alternating, oscillatory, and sector Hf-Zr zoning in kosnarite suggests local changes in physicochemical conditions during kosnarite growth (Fig. 1c, d). Therefore, the dominant oscillatory nanoscale zoning in kosnarite may be attributed either to cyclic changes in the Hf concentration in the parental hydrothermal fluid and/or non-equilibrium crystal growth with depletion in Hf^{4+} content in the adjacent solution that resulted in compositional gradients (Putnis et al. 1992; Shore and Fowler 1996; Stowell et al. 2011). Significant differences in the HfO_2 content in adjacent nanozones (22 vs. 7 wt.%) were observed in single crystal of kosnarite. This fact, in addition to the nanoscale size

(1–50-nm width) of the alternating Hf-rich zones, Hf-poor zones supports a non-equilibrium growth scenario. The observed sector and patchy zonings in kosnarite suggest that some of the crystals may have precipitated from separated batches of fluid under local equilibrium conditions, with selective partition of Hf and Rb and crystal growth rates exceeding the lattice diffusion rates (Watson and Liang 1995; Shtukenberg et al. 2009; Stowell et al. 2011). Therefore, it is unlikely that the oscillatory Hf zoning observed in kosnarite from the Chaquicocha deposit at Yanacocha is a result of rapid changes in fluid composition, pressure, and/or temperature as reported for oscillatory-zoned pyrites in fractured and sealed discontinuities in the deeper parts of other epithermal systems (Peterson and Mavrogenes 2014).

AQ11

Concluding remarks

The observations reported in this note document the first occurrence of kosnarite in hydrothermally altered volcanic rocks and point to the previously unforeseen role of phosphates in partitioning Hf, Zr, and Rb in areas of extensive acid leaching such as those occurring in epithermal systems, geothermal fields, and even porphyry deposits. Furthermore, (Hf,Zr)-phosphates may be of particular importance in geochemical studies attempting to understand the behavior of high-field strength elements (HFSE) in hydrothermal systems. Finally, potentially new geochronological applications of highly insoluble vein kosnarite, including Rb-Sr dating, may provide further age constraints in pervasively altered areas where other isotopic systems might have been reset.

Acknowledgments

The authors are grateful to Carl Henderson for the help with EMPA analyses conducted at the Electron Microbeam Analysis Laboratory (EMAL) at the University of Michigan. The comments by Atanas Hikov, Anthony Longo, Pietro Vignola, and Robert Linnen (Associate Editor) greatly improved the quality of the manuscript. Support for this study was provided by NSF EAR 052093 to Utsunomiya and Kesler. Financial support was provided by Japan Society of the Promotion of

Science (JSPS) to Utsunomiya. Martin Reich acknowledges support from FONDAP project 246 15090013, FONDECYT grant 1130030, and MSI grant Millennium Nucleus for Metal Tracing Along Subduction (NC130065).

References

Aja SU, Wood SA, Williams-Jones AE (1995) The aqueous geochemistry of Zr and the solubility of some Zr-bearing minerals. Appl Geochem 10:603–620

Bethke CM (1996) Geochemical reaction modelling: concepts and applications. Oxford University Press, New York

Birch WD, Pring A, Bevan K, Bevan DJM (1994) Wycheproofite: a new hydrated sodium aluminum zirconium phosphate from Wycheproof, Victoria, Australia, and a new occurrence of kosnarite. Mineral Mag 58:635–639

Birch WD, Pring A, Foord EE (1995) Selwynite, $NaK(Be,Al)Zr_2(PO_4)_4 \cdot 2H_2O$, a new gainesite-like mineral from Wycheproof, Victoria, Australia. Can Mineral 33:55–59

Brown P, Curti E, Grambow B (2005) Chemical thermodynamics of zirconium. Chemical Thermodynamics 8. Elsevier Science Publishers B.V, Amsterdam, https://www.oecd-nea.org/dbtdb/pubs/vol8-zirconium.pdf . Accessed 13 Aug 2014

Brownfield ME, Ford EE, Sutley SJ, Botinelly T (1993) Kosnarite. $KZr_2(PO_4)_3$, a new mineral from Mount Mica and Black Mountain, Oxford County, Maine. Am Mineral 78:653–656

Chouinard A, Williams-Jones AE, Leonardson AW, Hodgson CJ, Silva P, Tellez C, Vega J, Rojas F (2005) Geology and genesis of the multistage high-sulfidation epithermal Pascua Au-Ag-Cu deposit, Chile and Argentina. Econ Geol 100:463–493

Deditius AP, Utsunomiya S, Renock D, Ewing RC, Ramana CV, Becker U, Kesler SE (2008) A proposed new form of arsenian pyrite: composition, nanostructure and geochemical significance. Geochim Cosmochim Acta 72:2919–2933

Dill HG (2003) A comparative study of APS minerals of the Pacific Rim fold belts with special reference to South American argillaceous deposit. J S Am Earth Sci 16:301–320

Huminicki DMC, Hawthorne FC (2002) The crystal chemistry of the phosphate minerals. In: Kohn MJ, Rakovan J, Hughes JM (eds) Phosphates: geochemical, geobiological, and materials importance, 48. Rev Mineral Geochem, Mineralogical Society of America, Washington, DC, pp 123–253

Johnson JW, Oelkers EH, Helgeson HC (1992) SUPCRT92: a software package for calculating the standard molal thermodynamic properties of minerals, gases, aqueous species, and reactions from 1 to 5000 bar and 0 to 1000 °C. Comput Geosci 18:899–947

Linnen RL, Samson IM, Williams-Jones AE, Chakhmouradian AR (2014) Geochemistry of the rare-earth element, Nb, Ta, Hf, and Zr deposits. In: Holland H, Turekian K (eds) Treatise on geochemistry, second edition, vol 13:543–568

Longo AA (2000) The Carachugo-San Jose-Chaquicocha gold trend, Yanacocha district, northern Peru. In: Cluer JK, Price JG, Struhsacker EM, Hardyman RF, Morris CL (eds) Geology and ore deposits 2000, The Great Basin and Beyond, Geological Society of Nevada Symposium Proceedings, Reno/Sparks, Nevada, May 15–18, 2000, v. 1, p 201–220

Longo AA, Dilles JH, Grunder AL, Duncan R (2010) Evolution of calc-alkaline volcanism and associated hydrothermal gold deposits at Yanacocha, Peru. Econ Geol 105:1191–1241

Magdisov AA, Williams-Jones AE, van Hinsberg V, Salvi S (2011) An experimental study of the solubility of baddeleyite (ZrO_2) in

fluoride-bearing solutions at elevated temperature. Geochim Cosmochim Acta 75:7426–7434

More PB, Takaharu A, Steele IM, Swihart GH (1983) Gainesite, sodium zirconium beryllophosphate: a new mineral and its crystal structure. Am Mineral 68:1022–1028

Peterson EC, Mavrogenes JA (2014) Linking high-grade gold mineralization to earthquake-induced fault-valve processes in the Porgera gold deposit, Papua New Guinea. Geology 42:383–386

Putnis A, Fernandez-Diaz L, Prieto M (1992) Experimentally produced oscillatory zoning in the (Ba, Sr)SO4 solid solution. Nature 358:743–745

Rubin JN, Henry CD, Price JG (1993) The mobility of zirconium and other “immobile” elements during hydrothermal alteration. Chem Geol 110:29–47

Shore M, Fowler AD (1996) Oscillatory zoning in minerals: a common phenomenon. Can Mineral 34:1111–1126

Shtukenberg AG, Punin YO, Artamova OI (2009) Effect of crystal composition and growth rate on sector zoning in solid solutions grown from aqueous solutions. Mineral Mag 73:385–398

Simmons SF, White NC, John DA (2005) Geological characteristics of epithermal precious and base metal deposits. Econ Geol 100th Ann Vol. 1905–2005 100: 485–522

Stowell H, Zuluaga C, Boyle A, Bulman G (2011) Garnet sector and oscillatory zoning linked with changes in crystal morphology during rapid growth, North Cascades, Washington. Am Mineral 96:1354 –1362

Watson EB, Liang Y (1995) A simple model for sector zoning in slowly grown crystals: implications for growth rate and lattice

diffusion, with emphasis on accessory minerals in crystal rocks. Am Mineral 80:1179–1187